



Synthesis, characterization, and adsorption properties of *m*-aramid and chitosan hybrid composite films with the ratio of 100/0, 85/15, 65/35, 50/50, and 35/65 toward Hg(II) ions

Minghua Wang^a, Rongjun Qu^{a,*}, Changmei Sun^a, Yuzhong Niu^a, Ying Zhang^a,
Jingjing Gao^a, Honglan Cai^a, Xiquan Song^b

^aSchool of Chemistry and Materials Science, Ludong University, Yantai 264025, China, Tel. +86 135 8353 3866;
email: rongjunqu@sohu.com (R. Qu), Tel. +86 150 6638 7238; email: ytwmh@sohu.com (M. Wang)

^bYantai Tayho Advanced Materials Co., Ltd, Yantai 264006, China

Received 18 March 2018; Accepted 2 October 2018

ABSTRACT

Preparation of a series of novel hybrid composite materials *m*-aramid/chitosan to extract Hg(II) ions from water was carried out by using various weight ratios of *m*-aramid to chitosan (100/0, 85/15, 65/35, 50/50, and 35/65, respectively). Their structures were characterized by Fourier-transform infrared spectroscopy (FTIR) and scanning electron microscope. The result of FTIR indicated that the peak intensity of chitosan increases with increasing of the content of chitosan in the *m*-aramid/chitosan hybrid composite films. The adsorption properties of *m*-aramid/chitosan were affected by many factors including pH range, contact time, temperature, and the content of chitosan. The saturated adsorption capacity for Hg(II) ions increased with the increase of chitosan content and could reach to 0.09, 0.27, 0.43, 0.51, and 0.72 mmol·g⁻¹ at room temperature, respectively. The results show that the process of kinetic adsorption could be well described by the pseudo-second-order rate model. The isothermal adsorption experiments followed Langmuir and Freundlich models. Furthermore, the adsorption mechanism was also presumed.

Keywords: Hybrid composite; *m*-Aramid; Chitosan; Adsorption; Hg(II) ions

1. Introduction

With increasing industrialization including pigments, metallurgical processes, electroplating, mining, and leather industries, the contamination caused by heavy metals which entering the environment with the discharge of industrial wastewater became a serious environmental problem [1]. Heavy metals, particularly Hg(II) ions with two positive charges, are toxic and harmful to plants, animals, and human beings because of their toxicity and non-biodegradability. Many methods such as reverse osmosis, complexation, ion exchange, precipitation, and adsorption have been used to remove toxic metals from aqueous solution [2]. Among them, adsorption has attracted attention as an effective and

economical method for the removal of heavy metals from wastewater due to its low cost and simplicity. As a low-cost material, chitosan has proved to be an extremely promising adsorbent.

Chitosan, as a partially deacetylated derivative of the cheap, abundant, and renewable natural chitin [3], has been used in many biomedical applications, such as wound healing [4], wound dressing [5], food [6], enzyme immobilization [7], tissue engineering [8], and drug delivery [9] due to its antimicrobial activity, non-toxicity, biocompatibility, biodegradability, and excellent adsorption. It has been well known that chitosan and its derivatives can efficiently adsorb heavy metals from wastewater [10,11]. However, under acidic conditions, chitosan cannot remove metals directly because

* Corresponding author.

of the protonation of its $-NH_2$ groups. Up to the present, great attention have been paid to the chemical modification of chitosan through cross-linking, which was believed to be one of the most effective methods to avoid its protonation under acidic conditions, in which the linear structure of chitosan molecule could be transformed into network structure with the most commonly cross-linking agents, such as glutaraldehyde [12–14], glyoxal [15], epichlorohydrin [16,14], and genipin [17]. However, after cross-linking, activity sites of chitosan were reduced significantly because of the covalent interaction between cross-linking agents and chitosan, which would decrease the affinity of chitosan to metal ions [18–20]. In addition, little research has been carried out on the blend of chitosan and aramid fiber.

In recent years, aramid fiber has received considerable attention because of its unique properties such as low specific density and electrical conductivity, excellent resistance to thermal and chemicals, high tensile, and modulus strength [21]. Poly(*p*-phenyleneterephthalamide) (*p*-aramid) was known by its trade name Kevlar®, and poly(*m*-phenyleneisophthalamide) (*m*-aramid) was first described by Du Pont in 1961 [22] and commercialized in 1967, under the trademark Nomex® [22]. The *p*-aramid is the para-variety of aramid fiber and differs from its meta-variety *m*-aramid in the chemical structure only in phenylnitrogen and phenyl-carbonyl linkage positions [23] as shown in Fig. 1. *p*-Aramid is in wide use in the field of textile and advanced composites for many impact-related applications such as bulletproof vests, helmets, and various armor systems due to their outstanding strength to weight ratio and high tenacity, dimensional stability, high modulus, high strength, excellent heat, and flame resistant [24]. Unlike *p*-aramid, *m*-aramid is softer and more textile-like and is an inherently flame resistant and self-extinguishing polymer easier to process, resulting in more applications than *p*-aramid. Recently, *m*-aramid plays a vital role in the field of manufacturing protective garments worn at smelting furnaces or in oil refineries, portswear and racing wear, anti-static working clothing, heat-resistant gloves, and military heat-resistant protective clothing [25]. However, it should be noted that with the development of *m*-aramid industries comes the issue of waste fibers, which could cause severe environmental pollutions. Therefore, recycling and reusing of these wasted aromatic polyamide fibers are very urgent and important. As the development of membrane technology science [26,27], high value could be adopted by immobilized chitosan into the waste *m*-aramid to solve the problem of dissolution of chitosan in acidic solutions, thus the potential environmental pollutions could be avoided, and the waste could be reused as reinforcement materials to improve the chemical stability of *m*-aramid/chitosan composite films. It is quite simple to obtain acid-resistant composites by using the

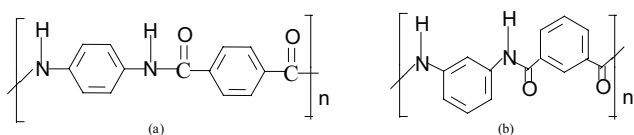


Fig. 1. (a) Poly(*p*-phenyleneterephthalamide) and (b) poly(*m*-phenyleneisophthalamide).

intermolecular hydrogen bond between them with aramid fibers being dissolved and physically mixed with chitosan.

Removal of heavy metals from aqueous solution has been the subject of extensive industrial research because they threaten not only the health of humans but also the environment [28]. To the best of our knowledge, it was found that the adsorption properties of *m*-aramid/chitosan hybrid composite films toward heavy metals were not reported. The objective of this study is to investigate the relationship between various weight ratios of adsorbents and their adsorption properties choosing Hg(II) ions as representative. In the present investigation, a series of *m*-aramid/chitosan hybrid composite films with various compositions (100/0, 85/15, 65/35, 50/50, and 35/65) were synthesized. The adsorbents were characterized by Fourier-transform infrared spectroscopy (FTIR) and scanning electron microscopy (SEM). Their adsorption capacities for Hg(II) ions were investigated. Furthermore, the effect of acidity, adsorption isotherm, and adsorption kinetics of Hg(II) ions adsorption were also studied.

2. Experiments

2.1. Materials and methods

Dimethylsulfoxide (DMSO, Damao Chemical Reagent Factory, Tianjin, China), methane sulfonic acid (CH_3SO_3H , Kelong Chemical Reagent Factory, Chengdu, China), and lithium chloride anhydrous (LiCl, Ruijinte Chemical Co., Ltd., Tianjin, China) were used as supplied. Chitosan (viscosity was 50–800 *mPa s*, degree of deacetylation was $\geq 90\%$) was obtained from Sinopharm Chemical Reagent Co., Ltd., China. *m*-Aramid was provided by Yantai Taiho Advanced Materials Co., Ltd., Yantai, China. Hg(II) ions stock solution was received from Huanqiu Reagent Factory, Jiangyan. All reagents were of analytical grade.

FTIR spectra were collected on a Nicolet MAGNAIR550 (series II) spectrophotometer within the range from 400 to 4,000 cm^{-1} . The morphology and thickness of hybrid composite material *m*-aramid/chitosan were determined on a field emission SEM (Hitachi S-4800 SEM, Japan). The concentration of Hg(II) ions was determined with a flame atomic absorption spectrophotometer (Model 932A, GBC, Australia).

2.2. Preparation of *m*-aramid/chitosan hybrid composite film

The preparation of *m*-aramid/chitosan hybrid composite film is similar to the method described in a study by Kim and Lee [29]: *m*-aramid was sequentially washed three times with distilled water ($\sim 60^\circ C$), ethanol, and acetone, and then dried overnight at room temperature. A total of 10 g of *m*-aramid was added to 100 mL of DMSO with 10 g of LiCl to produce a homogeneous 10 wt% *m*-aramid solution with constant stirring at $130^\circ C$ for 4 h. Chitosan (1.5 g), distilled water (100 mL), and 1 g of methane sulfonic acid were added to a flask and stirred for 1 h at room temperature followed by freeze-drying for 48 h. In total, 10 g of freeze-dried chitosan–methane sulfonic acid salt and 100 mL of DMSO were added to a three-necked flask, and the mixture was stirred at room temperature for 1 h. A total of five different solutions were made with the following ratios of *m*-aramid and chitosan–methane sulfonic acid salt by weight: 100/0, 85/15, 65/35,

50/50, and 35/65 and were stirred for 2 h at 60°C. The five solutions were coagulated on film-making plates in a 1% sodium hydroxide solution bath at room temperature for 6 h, washed with abundant distilled water, soaked in distilled water at room temperature for 6 h and at 80°C for 20 min, and then dried at room temperature.

2.3. Saturated adsorption

Into a conical flask with *m*-aramid/chitosan hybrid film (0.25 g), 20 mL of Hg(II) ions solution (pH 2.06) with an initial concentration (C_0) of 0.002 mol·L⁻¹ were added. After the flask was shaken at room temperature for 24 h, and then filtered off, the final Hg(II) ions solution concentration was analyzed with atomic adsorption spectrometry (AAS). The adsorption amount (Q : mmol·g⁻¹) of Hg(II) ions was calculated according to Eq. (1).

$$Q = \frac{(C_0 - C)V}{W} \quad (1)$$

where C_0 and C (mmol·mL⁻¹) are the initial and equilibrium concentrations of Hg(II) ions, respectively; V (mL) is the volume of Hg(II) ions solution, and W (g) is the dry weight of *m*-aramid/chitosan blend film.

2.4. Effect of pH

Effect of pH on the adsorption of Hg(II) ions has been investigated in the pH range of 1–5 with HNO₃ and hexamethylenetetramine to adjust the acidity of medium. In total, 20 mg of *m*-aramid/chitosan with 20 mL of Hg(II) ions solution (0.001 mol·L⁻¹) were shaken for 20 h at room temperature. Then, the adsorption of Hg(II) ions was examined.

2.5. Adsorption isotherm

Isothermal adsorption experiments were carried out as following: the initial Hg(II) ions concentration was varied from 0.005 to 0.02 mol·L⁻¹ with 20 mg of *m*-aramid/chitosan after 24 h of shaking. The sample was filtered before AAS measurement.

2.6. Adsorption kinetics

A total of 50 mg of adsorbent with 25 mL of Hg(II) ions solution (0.02 mol·L⁻¹) were shaken at different temperatures (10°C, 15°C, 25°C, and 35°C), respectively. And, 1 mL of supernatant solution was taken from the conical flask at different time intervals and the concentration of Hg(II) ions was measured with AAS.

2.7. The rate of weight loss

After 50 mg of sample was immersed in 50 mL of 1% acetic acid solution, the samples were shaken for different times. After the surface solution on the hybrid film was removed with filter paper, the material was dried at 105°C for 24 h.

The rate of weight loss (WL) was calculated according to Eq. (2).

$$W_L = \frac{W_0 - W_1}{W_0} \times 100\% \quad (2)$$

where W_0 and W_1 are sample weights before and after soaking in 1% acetic acid solution, respectively.

3. Results and discussion

3.1. FTIR characterization

FTIR spectra of the pure *m*-aramid and *m*-aramid/chitosan hybrid films are shown in Fig. 2. Peaks at 3,305, 1,656, 1,609, and 1,541 cm⁻¹ were due to N–H stretching vibration, amide C=O stretching, C=C stretching vibration of the aromatic ring, and N–H in-plane bending modes of *m*-aramid, respectively [29].

The characteristic peaks of chitosan, C–H stretching vibration at 2,882 cm⁻¹ and stretch vibration of C–O bond at 1,085 and 1,034 cm⁻¹ [10], could still be observed obviously along with the characteristic absorption peaks of *m*-aramid after the incorporation of chitosan into *m*-aramid, and the intensity was increased with the increase of the ratio of chitosan, which indicated a good compatibility between *m*-aramid and chitosan.

Chitosan, having two hydroxyl groups (–OH) and one amine group (–NH₂), and *m*-aramid having one amide group in each repeating unit, have four types of intermolecular hydrogen bond between them [30] as shown in Fig. 3.

3.2. Morphology characterization

Morphology, shape, and cross-section of pure *m*-aramid and hybrid films were characterized with SEM. Surface images of films are shown in Fig. 4. SEM images showed that the aggregation of particles in *m*-aramid film was about 50–250 nm in size, and the 35/65 wt% *m*-aramid/chitosan hybrid film had pores with diameter of 0.1–5 μm, indicating that even in the same coagulation system, the mixed liquor might have different coagulation forms [29]. Moreover, the pure chitosan became transparent when it was coagulated

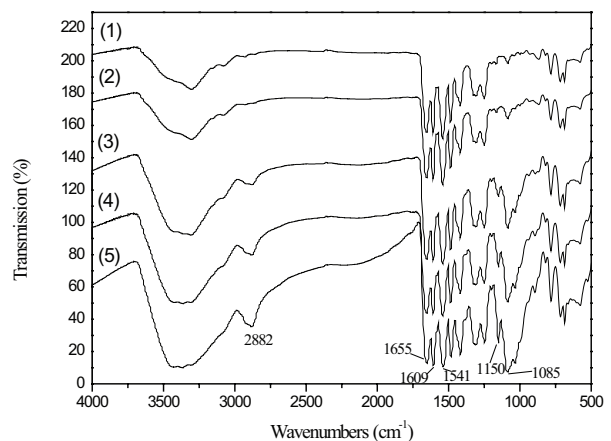


Fig. 2. FTIR spectra of pure *m*-aramid and *m*-aramid/chitosan films, (1) pure *m*-aramid, (2) 85/15, (3) 65/35, (4) 50/50, and (5) 35/65 wt %.

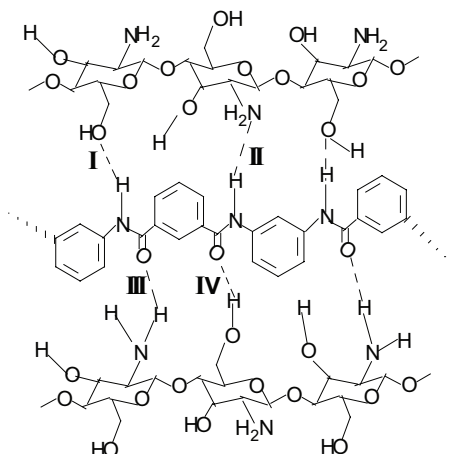


Fig. 3. Four types of intermolecular hydrogen bond between *m*-aramid and chitosan.

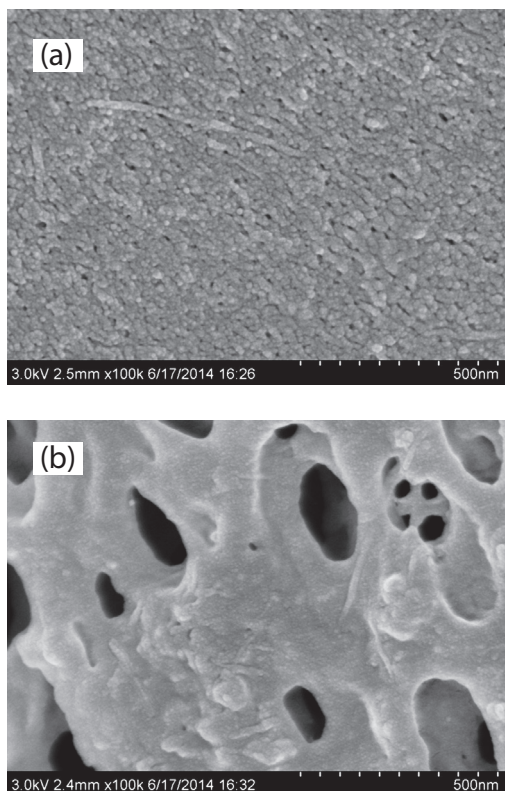


Fig. 4. Surface images of *m*-aramid/chitosan hybrid films: (a) 100/0 and (b) 35/65 wt%.

in 1% NaOH solution, whereas, the pure *m*-aramid and four *m*-aramid/chitosan films were opaque, which could be attributed to the mass of small voids in the structure formed during coagulation.

Cross-sectional SEM images of films are shown in Fig. 5. The cross-sectional SEM images of the films were obtained after freezing with liquid nitrogen followed by breaking. Fig. 5 shows that both of the two films have three-dimensional porous structures. The cross-sectional image of pure *m*-aramid film had a relatively smooth surface,

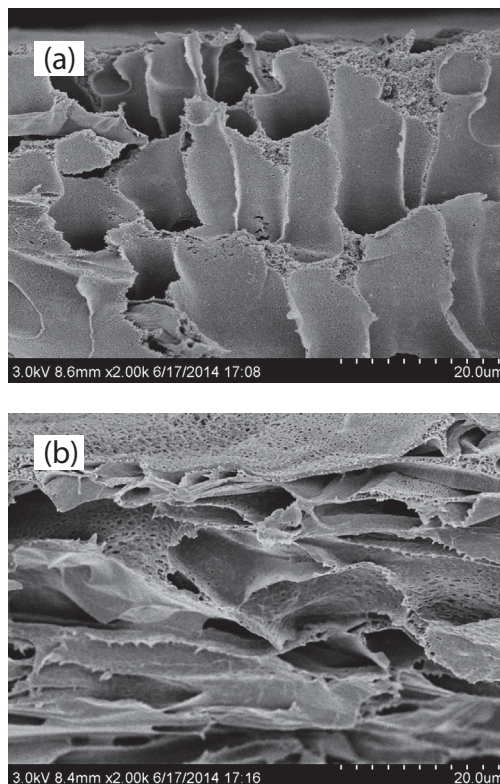


Fig. 5. Cross-sectional SEM images of *m*-aramid/chitosan films: (a) 100/0 and (b) 35/65 wt%.

meanwhile, the 35/65 wt% *m*-aramid/chitosan hybrid film contained more micropores on the wall of macropores, and the pore sizes were all from nanometers to 10 μm in these two dense sponge-like structures probably because of their different coagulation rates. Figs. 4 and 5 also show that chitosan adhered to *m*-aramid very well without phase separation, which indicated the phase compatibility between *m*-aramid and chitosan. The results showed that chitosan had a good compatibility to *m*-aramid, and these hybrid films were very stable.

3.3. Rate of WL

As shown in Fig. 6, the ratio of *m*-aramid/chitosan had a significant influence on their WL. Except for *m*-aramid, the rate of WL of all hybrid materials was increased along the time and reached the maximum value at about 1.5 h. The film with more chitosan had a higher WL rate than that with less chitosan. WL rates of 85/15, 65/35, 50/50, and 35/65 were 0.46%, 0.82%, 2.99%, and 6.15%, respectively, suggesting that the optimal ratio of *m*-aramid/chitosan film was 50/50 to adsorb metal ions.

3.4. Static saturated adsorption capacity

Batch adsorption experiments were performed to remove Hg(II) ions by the synthesized *m*-aramid/chitosan hybrid films. The hybrid membrane without acid treatment, after adsorbing Hg(II) ions, had no chitosan loss. The saturated adsorption capacities of these *m*-aramid/chitosan films

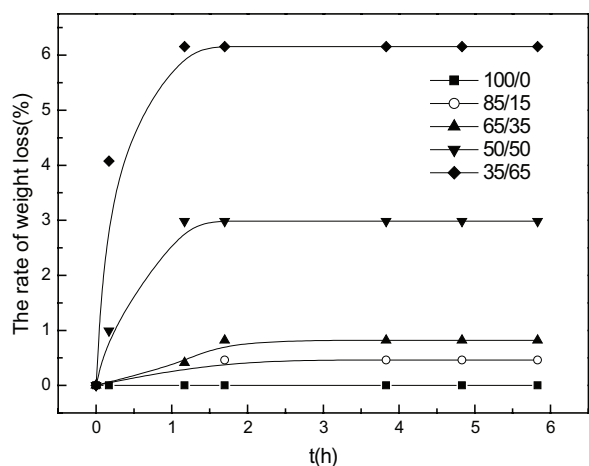


Fig. 6. Rates of weight loss of *m*-aramid/chitosan hybrid films in 1% acetic acid solution.

with the ratio of 100/0, 85/15, 65/35, 50/50, and 35/65 were calculated. As shown in Fig. 7, the saturated adsorption capacity for Hg(II) ions could reach 0.09, 0.27, 0.43, 0.51, and 0.72 mmol·g⁻¹ at room temperature, respectively, with the order of 35/65 > 50/50 > 65/35 > 85/15 > 100/0. With the increase of the chitosan content, adsorption capacity of the hybrid film was obviously increased, probably because of amine and hydroxyl groups in chitosan, the main active sites for metal ions. However, the utilization ratio of chitosan of 85/15, 65/35, 50/50, and 35/65 was 1.83, 1.23, 1.02, and 1.11, respectively, indicating that a higher chitosan content did not ensure a higher utilization ratio of chitosan in the hybrid film because the effect of hydrogen bonds was diminished and the rate of WL of chitosan was increased with the increase of chitosan content.

Chitosan has been modified by other researchers to increase adsorption capacity. It had been reported that Rodrigo et al. [14] synthesized epichlorohydrin-crosslinked and glutaraldehyde-crosslinked chitosan membranes with the maximum adsorption capacity of 30.3 and 75.5 mg·g⁻¹ (0.15 and 0.37 mmol·g⁻¹), respectively. It could be observed that most of *m*-aramid/chitosan films exhibited better adsorption capacity than those chitosan membranes. It was reported that two chitosan films were obtained using chitosan cross-linked with genipin (Chg) and then grafted with caffeic acid (Chg+caf) by Rocha et al [17]. The estimated capacity of Chg and Chg+caf films was 2.2 and 4.0 mg·g⁻¹ (0.011 and 0.020 mmol·g⁻¹), respectively. The adsorption capacity values of *m*-aramid/chitosan films were also higher than those mentioned above.

3.5. Effect of pH

In order to investigate the function of *m*-aramid/chitosan films, the adsorption capacities for Hg(II) ions at different pH conditions value were determined and are shown in Fig. 8. It could be observed that all kinds of *m*-aramid/chitosan films exhibit good adsorption capacity for Hg(II) ions, indicating that the films might be used to adsorb Hg(II) ions from wastewater. The adsorption capacities of adsorbents increased with the increasing of chitosan content of *m*-aramid/chitosan

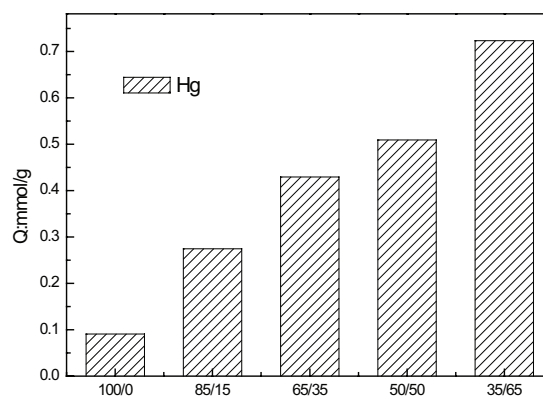


Fig. 7. Adsorption of Hg(II) ions by *m*-aramid/chitosan hybrid films with the initial pH value of 2.76.

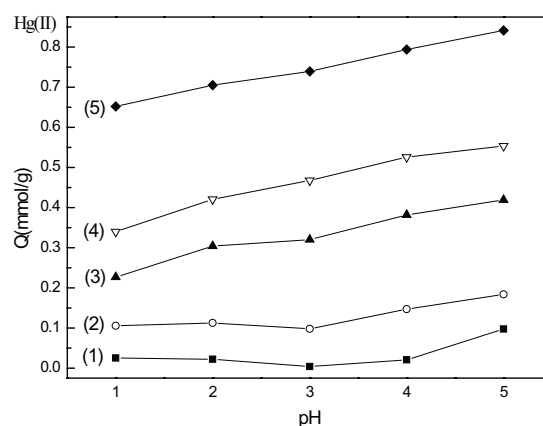


Fig. 8. Effects of initial pH on Hg(II) ions adsorption capacities of materials: (1) the pure *m*-aramid, (2) 85/15, (3) 65/35, (4) 50/50, and (5) 35/65 wt%.

films due to the increasing of functional groups because the higher content of functional groups of chitosan gave rise to better coordination with Hg(II) ions.

As shown in Fig. 8, pH had a slight effect on the Hg(II) ions adsorption of *m*-aramid/chitosan hybrid films if the content of chitosan was less than 15%. Adsorption capacities for Hg(II) ions were increased with the increase of pH when the content of chitosan was higher than 35%. The adsorption amount could reach to the maximum at pH = 5 because the Hg(II) ions hydrolysis might occur when pH was above 5. Hg(II) ions is the dominant species when pH is below 5.5, which can be bound on *m*-aramid/chitosan films through coordination, while the main form is Hg(OH)₂ when pH is above 5.5 [28]. On the other hand, the electrostatic repulsion between Hg(II) ions and the protonated groups or H⁺ ion might result in the decrease of Hg(II) ions adsorption when pH was decreased, therefore decreasing the Hg(II) ions removal efficiency [31,32]. Fig. 8 also shows the uptake of Hg(II) ions increased with an increasing content of chitosan.

3.6. Adsorption isotherm

As shown in Fig. 9, the Hg(II) ions adsorption capacity was increased with the increase of Hg(II) ions concentration

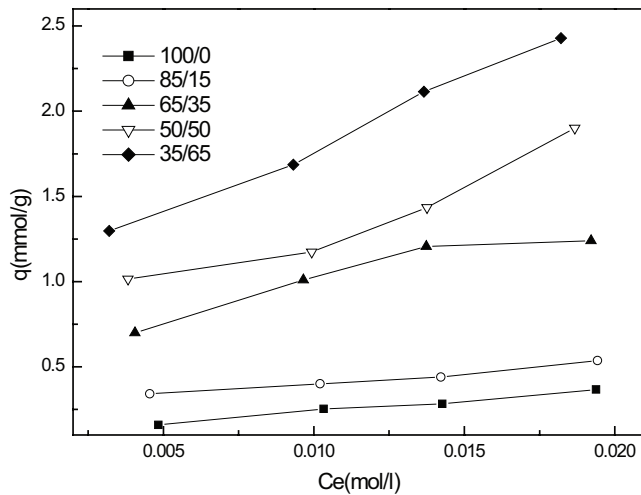


Fig. 9. Hg(II) ions adsorption isotherms of *m*-aramid/chitosan films at room temperature.

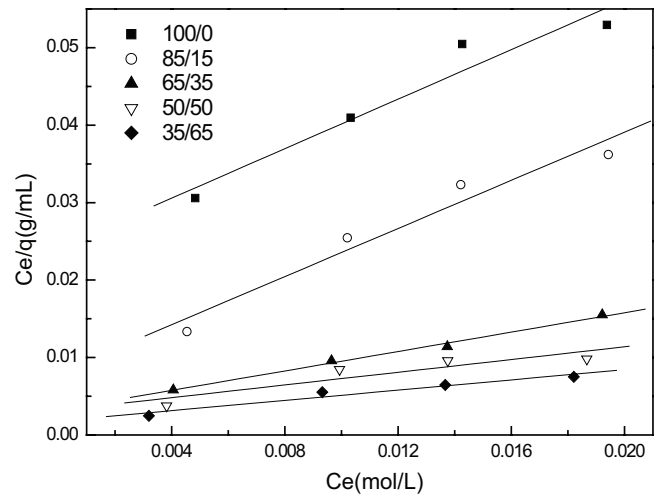


Fig. 10. Hg(II) ions Langmuir isotherms of *m*-aramid/chitosan films.

and the chitosan ratio. The isothermal equilibrium data were processed in terms of Langmuir [33] and Freundlich [34] isotherm models according to the following equations:

$$\frac{C_e}{q_e} = \frac{C_e}{q_0} + \frac{1}{q_0 b} \quad (3)$$

$$\ln q_e = \ln K_F + \frac{1}{n} \ln C_e \quad (4)$$

where q_e and q_0 are the adsorption capacity and theoretical saturation adsorption capacity of the adsorbent ($\text{mmol}\cdot\text{g}^{-1}$), C_e is the equilibrium concentration of Hg(II) ions ($\text{mmol}\cdot\text{L}^{-1}$), b is the Langmuir adsorption constant ($\text{mL}\cdot\text{mmol}^{-1}$), K_F is the Freundlich constant ($\text{mmol}\cdot\text{g}^{-1}$), and n is the Freundlich exponent related to adsorption intensity.

Linear Langmuir and Freundlich adsorption isotherms of Hg(II) ions were obtained as shown in Figs. 10 and 11, respectively. The q , b , $1/n$, K_F values, and the linear regression correlation coefficients (R_L^2 and R_F^2) for Langmuir and Freundlich isotherms are listed in Table 1. Results showed that the regression coefficients (R_L^2) of Langmuir model and (R_F^2) Freundlich model were close to 1, indicating that Langmuir and Freundlich models could well interpret the adsorption of *m*-aramid/chitosan hybrid films for Hg(II) ions, that is, the adsorption of Hg(II) ions onto *m*-aramid/chitosan hybrid films in aqueous medium should belong to a monomolecular layer [35]. In addition, $1/n$ values of Hg(II) ions from Freundlich isotherm model were all less than 1, implying that the marginal adsorption energy was decreased with the increase of the surface Hg(II) ions concentration and the Hg(II) ions could be favorably adsorbed by *m*-aramid/chitosan hybrid films.

3.7. Adsorption kinetics

As shown in Fig. 12, the adsorption increased sharply within the beginning of 1 h and then the adsorption

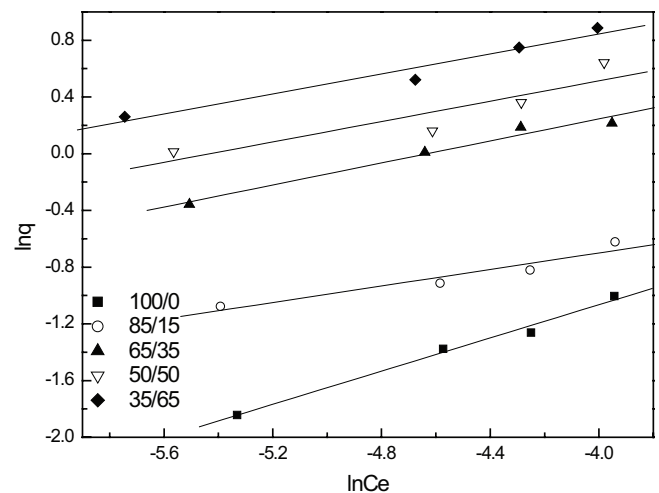


Fig. 11. Hg(II) ions Freundlich isotherms of *m*-aramid/chitosan films.

equilibrium was reached within approximately 4 h, probably, not only due to the strong chelation and good affinity of Hg(II) ions onto *m*-aramid/chitosan films, but also the small diffusion barrier in the resin layer. The uptake-time curves show that the maximum uptaking equilibrium increased with the increase of temperature, indicating that the Hg(II) ions adsorption was an endothermic process. The adsorbing rate did not always increase with the increase in temperature within half an hour, indicating the diffusion rate of Hg(II) ions might be enhanced by the increase of temperature and quickly forms complexes on the outer layer. The higher steric hindrance at higher temperature could slow down the diffusing rate of Hg(II) ions into the inside of the adsorbents to combine with active sites. Moreover, the order of adsorption capacities of Hg(II) ions onto *m*-aramid/chitosan films was in accordance with that obtained in section of static saturated adsorption capacity.

The adsorption progress of solution and adsorbed phases in adsorbate–adsorbent systems could be described

Table 1
Langmuir and Freundlich parameters of *m*-aramid/chitosan films toward Hg(II) ions at room temperature

Adsorbent wt%	Langmuir			Freundlich		
	q (mmol·g ⁻¹)	b (mL·mmol ⁻¹)	R_L^2	K_F (mmol·g ⁻¹)	$1/n$	R_F^2
100/0	0.414	1.51	0.9692	1.796	0.783	0.9946
85/15	1.247	0.516	0.9758	1.338	0.149	0.9590
65/35	3.077	0.519	0.9967	1.475	0.556	0.9863
50/50	3.155	0.772	0.9116	1.432	0.513	0.9071
35/65	5.495	0.550	0.9751	1.423	0.443	0.9775

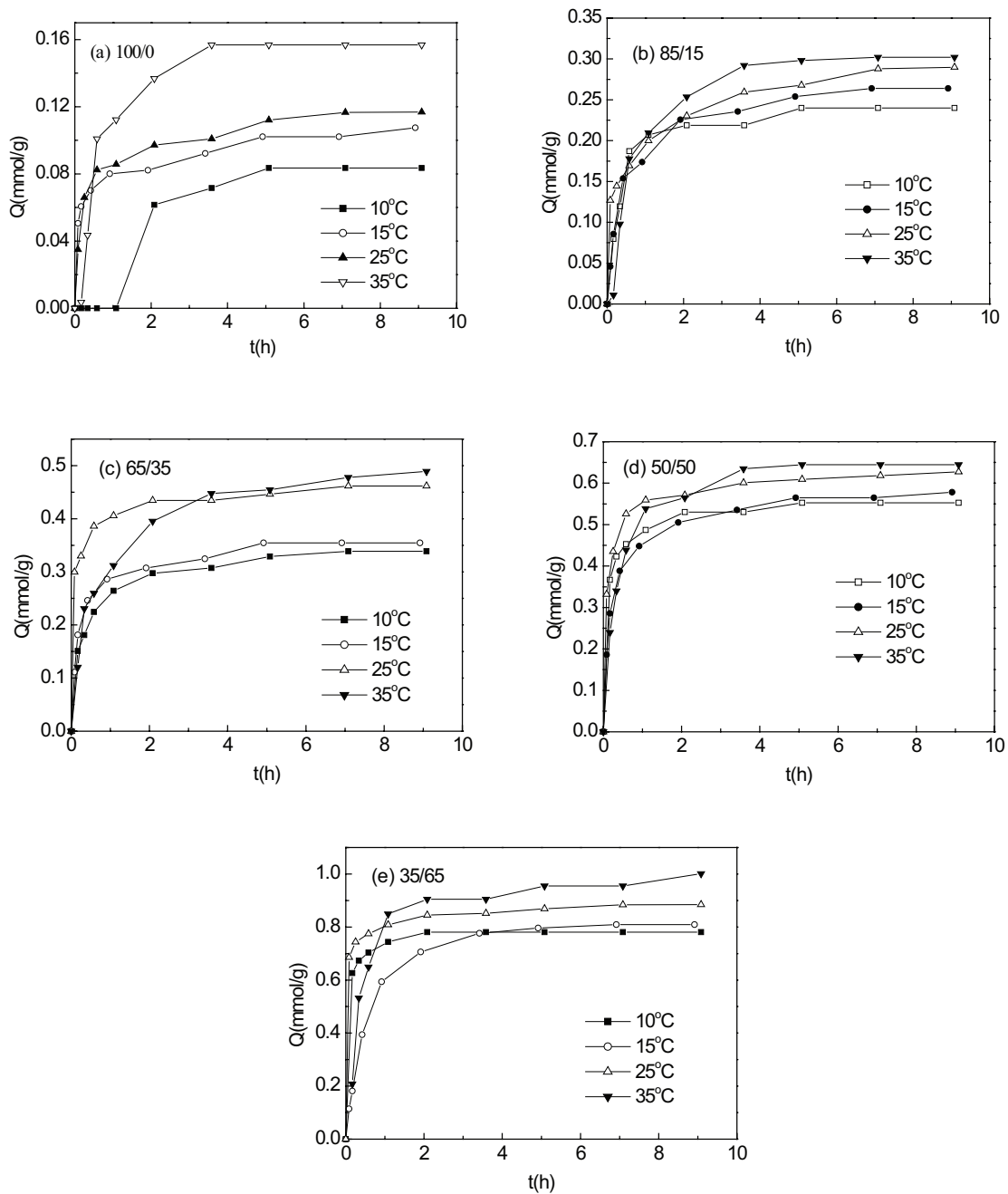


Fig. 12. Hg(II) ions adsorption kinetics of *m*-aramid/chitosan films at different temperatures: (a) 100/0, (b) 85/15, (c) 65/35, (d) 50/50, and (e) 35/65 wt% (the initial concentration of Hg(II) ions: 0.02 mol·L⁻¹; adsorbent material: 50 mg).

as follows [36–38]: (1) bulk diffusion, Hg(II) ions transported from the bulk solution to the boundary film; (2) film diffusion, Hg(II) ions transferred from the boundary film to the outer surface of the *m*-aramid/chitosan film; (3) intraparticle diffusion, Hg(II) ions transferred from surface into the inner of matrix of adsorbents; and (4) chelation on active sites. The diffusion steps of Hg(II) ions onto the *m*-aramid/chitosan hybrid films are shown in Fig. 13.

Because of vigorous stirring, the first step could be ignored at the low Hg(II) ions concentration. The last step could also be neglected because the chelation could occur rapidly. Therefore, only film diffusion and intraparticle diffusion were considered as the rate-controlling steps. In order to distinguish film diffusion and intraparticle diffusion, several models had been studied. As Guibal et al. [39] described, the shape (tablet rather than sphere) and porosity (weak porosity) of chitosan were very different from conventional materials. A linear fit of experimental data according to several simplified kinetic models is listed in Table 2 [39]: (1) the homogeneous diffusion model controlled by film diffusion (HDM-FD); (2) the homogeneous diffusion model controlled by particle diffusion (HDM-PD); (3) the shrinking core model controlled by film diffusion (SCM-FD); (4) the shrinking core model controlled by particle diffusion (SCM-PD); and (5) the shrinking core model controlled by chemical reaction (SCM-CR).

The HDM-FD and HDM-PD were used to match the adsorption kinetics of *m*-aramid/chitosan films for Hg(II) ions, and the linearization of kinetics data is shown in Fig. 14. The linear equation and correlation coefficient of HDM-FD and HDM-PD are listed in Tables 3 and 4, respectively. These results show that, according to coefficient values (R^2) of HDM-FD and HDM-PD, both HDM-FD and HDM-PD fitted with kinetic data of Hg(II) ions adsorption onto *m*-aramid/chitosan films.

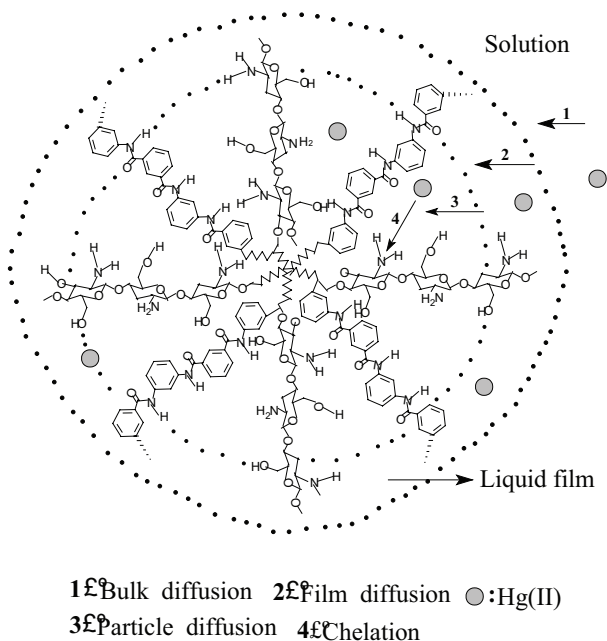


Fig. 13. Diffusion steps of Hg(II) ions onto *m*-aramid/chitosan hybrid film.

According to the theory of hard and soft acids and bases, Hg(II) ions were soft ions and can form strong bonds with nitrogen atom of amino group except that $-\text{OH}$ also take part in the adsorption [40], which was confirmed by Chen and Wang [10]. Furthermore, Braier and Jishi [41] also proposed that the sorption of metal ions took place in the vicinity of the glycosidic oxygen with contributions from nitrogen and $-\text{OH}$ groups. Therefore, the structure of Hg(II) ions onto the *m*-aramid/chitosan films could be proposed as shown in Fig. 15.

3.8. Adsorption kinetics model

In order to investigate the sorption mechanism for the adsorption of Hg(II) ions by *m*-aramid/chitosan films, two simplified pseudo-first-order and pseudo-second order models were used as the following Eqs. (5) and (6), respectively [42,43].

$$\log(q_e - q_t) = \log q_e - \frac{k_1}{2.303} t \quad (5)$$

$$\frac{t}{q_t} = \frac{1}{k_2 q_e^2} + \frac{1}{q_e} t \quad (6)$$

where q_e and q_t are adsorbed amounts ($\text{mmol}\cdot\text{g}^{-1}$) at equilibrium and at time t (h), respectively; k_1 (h^{-1}) and k_2 ($\text{g}\cdot\text{mmol}^{-1}\cdot\text{h}^{-1}$) are the rate constants of pseudo-first-order and pseudo-second-order adsorption.

Pseudo-first-order kinetic and pseudo-second-order kinetic models of *m*-aramid/chitosan films for Hg(II) ions adsorption are shown in Fig. 16, and the results are listed in Table 5. According to results from Azizian [44], with high initial concentration of solute, the general equation converts to a pseudo-first-order model, while it converts to a pseudo-second-order model at lower initial concentration of solute. The correlation coefficient (R^2) values of pseudo-second-order kinetic model were higher than those from the pseudo-first-order kinetic model, suggesting that the process of kinetic adsorption could be better described with the pseudo-second-order kinetic rate model. Therefore,

Table 2
Linearization of kinetic data-simplified equations for ion-exchange mechanisms with HDM and SCM controlled by FD, PD, and CR (X is the fractional approach to equilibrium)

Model and controlling step	$F(X)$, y -axis	x -axis
HDM-FD	$-\ln(1-X)$	t
HDM-PD	$-\ln(1-X^2)$	T
SCM-FD	X	$\int_0^t C(t) dt$
SCM-PD	$3-3(1-X)^{2/3}-2X$	$\int_0^t C(t) dt$
SCM-CR	$1-(1-X)^{1/3}$	$\int_0^t C(t) dt$

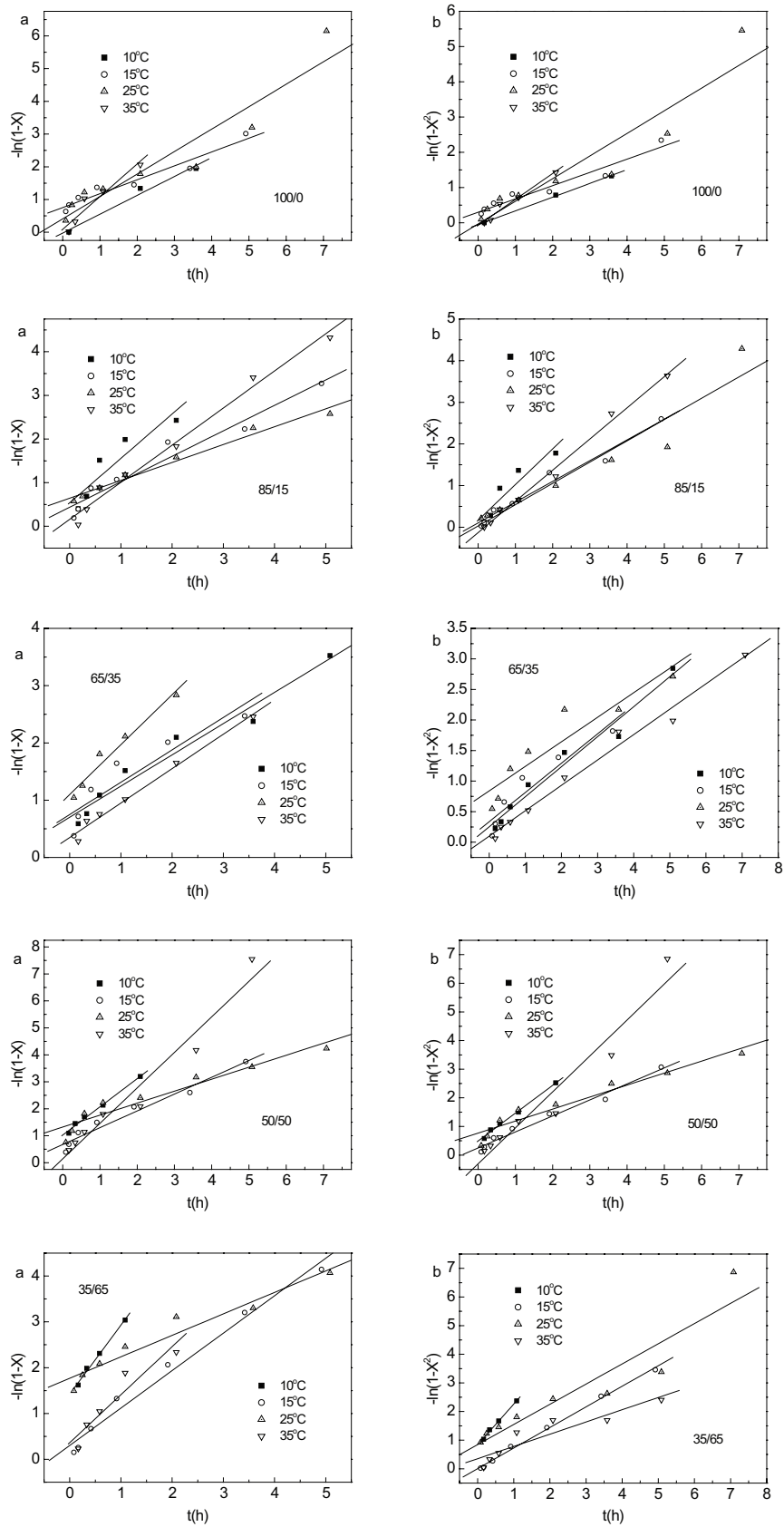


Fig. 14. Linearization of kinetics data of *m*-aramid/chitosan films for Hg(II) ions: (a) homogeneous diffusion model controlled by film diffusion ((HDM-FD) and (b) homogeneous diffusion model controlled by particle diffusion ((HDM-PD).

Table 3
Parameters of HDM-FD

Resins	T (°C)	Linear equation	R ²	Intercept error
100/0	10	$y = -0.02455x + 0.5761$	0.9899	0.08253
	15	$y = 0.7549x + 0.4241$	0.9741	0.04403
	25	$y = 0.4069x + 0.6857$	0.9505	0.09155
	35	$y = 0.09119x + 0.9977$	0.9580	0.1725
85/15	10	$y = 0.5389x + 1.0171$	0.9198	0.2505
	15	$y = 0.4363x + 0.5836$	0.9769	0.05705
	25	$y = 0.6428x + 0.4098$	0.9904	0.02554
	35	$y = 0.1577x + 0.8486$	0.9929	0.04522
65/35	10	$y = 0.7011x + 0.5453$	0.9797	0.04996
	15	$y = 0.7490x + 0.5651$	0.9253	0.1158
	25	$y = 1.0989x + 0.8713$	0.9825	0.09547
	35	$y = 0.3492x + 0.6006$	0.9931	0.03547
50/50	10	$y = 1.0259x + 1.0453$	0.9954	0.05822
	15	$y = 0.6737x + 0.6234$	0.9817	0.05396
	25	$y = 1.3148x + 0.4448$	0.9579	0.05446
	35	$y = 0.1343x + 1.3182$	0.9766	0.1299
35/65	10	$y = 1.4232x + 1.5041$	0.9969	0.08345
	15	$y = 0.3013x + 0.8197$	0.9915	0.04806
	25	$y = 1.7675x + 0.4687$	0.9700	0.05253
	35	$y = 0.3616x + 1.0478$	0.9481	0.2028

Table 4
Parameters of HDM-PD

Resins	T (°C)	Linear equation	R ²	Intercept error
100/0	10	$y = -0.0533x + 0.3900$	0.9994	0.01352
	15	$y = 0.3001x + 0.3764$	0.9724	0.0404
	25	$y = -0.03348x + 0.6423$	0.9418	0.09361
	35	$y = -0.0717x + 0.7350$	0.9835	0.07798
85/15	10	$y = 0.1695x + 0.8548$	0.9371	0.1839
	15	$y = 0.1042x + 0.4983$	0.9865	0.03697
	25	$y = 0.0313x + 0.5108$	0.9598	0.06102
	35	$y = -0.1271x + 0.7491$	0.9961	0.02967
65/35	10	$y = 0.2526x + 0.4914$	0.9834	0.04061
	15	$y = 0.3347x + 0.4794$	0.9475	0.08091
	25	$y = 0.8387x + 0.402$	0.9345	0.06851
	35	$y = 0.09614x + 0.4161$	0.9924	0.02111
50/50	10	$y = 0.4928x + 0.9714$	0.9968	0.04508
	15	$y = 0.2485x + 0.5596$	0.9890	0.03739
	25	$y = 0.7686x + 0.4190$	0.9675	0.04472
	35	$y = -0.3042x + 1.2560$	0.9711	0.1381
35/65	10	$y = 0.8364x + 1.4235$	0.9977	0.06824
	15	$y = 0.00394x + 0.7194$	0.9984	0.01843
	25	$y = 0.8431x + 0.7049$	0.9426	0.1020
	35	$y = 0.3525x + 0.4276$	0.9258	0.07811

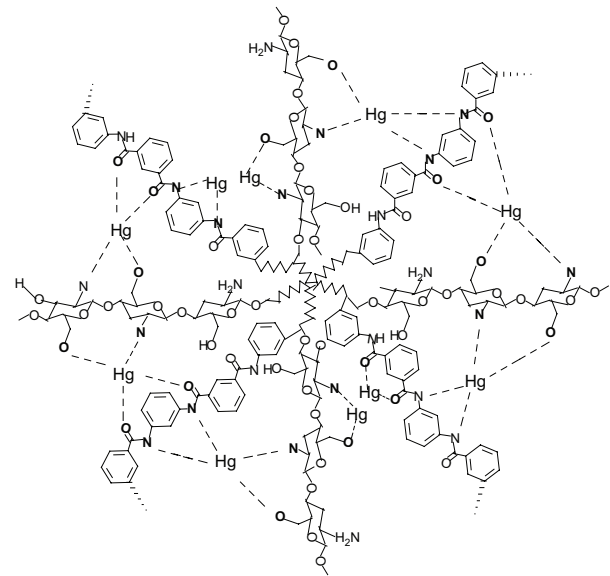


Fig. 15. The proposed structure of Hg(II) ions on *m*-aramid/chitosan film.

these new materials had great potential as adsorbents to remove Hg(II) ions from water with lower metal initial concentration.

4. Conclusions

A series of novel *m*-aramid/chitosan films with the ratio of 100/0, 85/15, 65/35, 50/50, and 35/65 were successfully prepared and systematically characterized with FTIR and SEM techniques.

It was found that the adsorption abilities of *m*-aramid/chitosan toward Hg(II) ions were dependent on pH value of solution and the optimum pH was 5. Their Hg(II) ions adsorption capabilities were increased with the increase of the chitosan content and temperature. However, the higher content of chitosan did not ensure the high utilization ratio of chitosan.

Regarding to adsorption thermodynamics and kinetics of Hg(II) ions on *m*-aramid/chitosan films, the Langmuir and Freundlich models could be used to describe the Hg(II) ions adsorption on *m*-aramid/chitosan films. The kinetic adsorption process could also be well described with the pseudo-second-order rate model in which the film diffusion might be the primary rate-determining step along with partly particle diffusion. The *m*-aramid/chitosan films with low chitosan content showed a slow WL rate than those with high chitosan content.

Acknowledgments

The authors are grateful for the financial support provided by the National Natural Science Foundation of China (Grant Nos. 51673089, 51373074, 51073075, 51302127, and 51143006), Scientific and Technological Research Program of Shandong province (No. 2014GGX102027), and the Industry, Education and Research Cooperative Education Project of Ministry of Education of China (No. 201702068013).

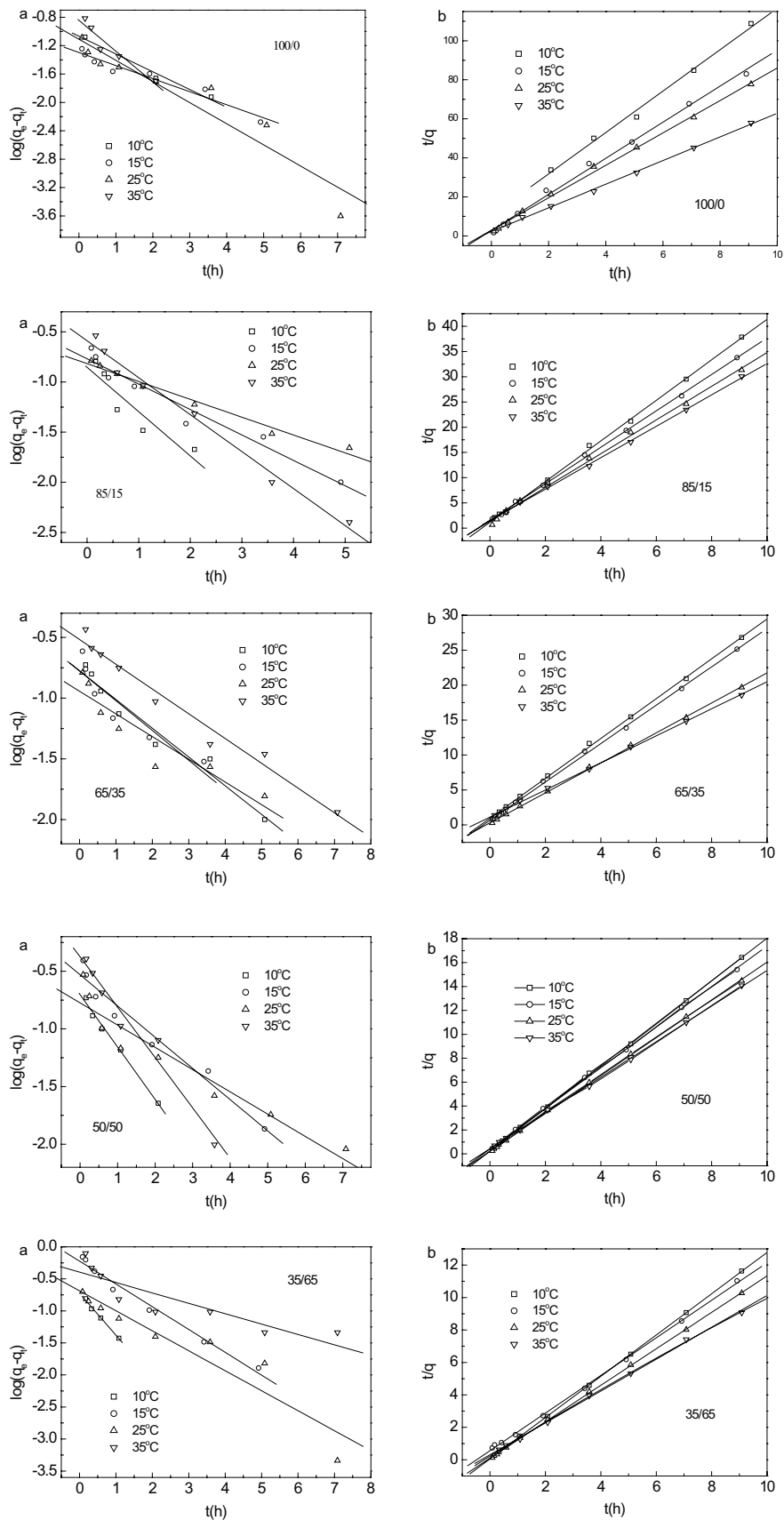


Fig. 16. (a) Pseudo-first-order kinetic model and (b) pseudo-second-order kinetic model of *m*-aramid/chitosan films for Hg(II) ions.

Table 5
Adsorption kinetic parameters of *m*-aramid/chitosan films for Hg(II) ions at different temperatures

Resin	<i>T</i> (°C)	Pseudo-first-order kinetics			Pseudo-second-order kinetics		
		k_1 (h ⁻¹)	$q_{e, cal}$ (mmol·g ⁻¹)	R_1^2	k_2 (g mmol ⁻¹ h ⁻¹)	$q_{e, cal}$ (mmol·g ⁻¹)	R_2^2
100/0	10	2.459	0.562	0.9899	10.513	0.0947	0.9970
	15	2.986	0.654	0.9741	0.852	0.356	0.9980
	25	2.554	0.504	0.9505	1.038	0.340	0.9987
	35	1.944	0.369	0.9580	0.827	0.447	0.9994
85/15	10	1.966	0.362	0.9198	0.354	0.838	0.9995
	15	1.768	0.558	0.9769	0.691	0.633	0.9996
	25	1.882	0.664	0.9904	0.574	0.722	0.9985
	35	1.355	0.428	0.9930	0.734	0.662	0.9996
65/35	10	1.784	0.580	0.9797	0.318	1.050	0.9997
	15	1.786	0.568	0.9253	0.157	1.525	0.9996
	25	2.171	0.650	0.9277	0.0395	3.435	0.9998
	35	1.190	0.625	0.9875	0.651	0.891	0.9996
50/50	10	1.619	0.352	0.9954	0.0296	4.351	0.9999
	15	1.222	0.536	0.9818	0.101	2.414	0.9997
	25	1.781	0.641	0.9579	0.0315	4.478	0.9999
	35	0.863	0.366	0.9819	0.129	2.278	0.9998
35/65	10	1.671	0.222	0.9969	0.101	2.489	0.9999
	15	0.513	0.441	0.9915	0.273	1.779	0.9996
	25	1.581	0.488	0.9453	0.0415	4.629	0.9999
	35	0.909	0.688	0.8874	0.0976	3.230	0.9994

References

- [1] B. Hassan, V.K. Rajan, V.M.A. Mujeeb, K. Muraleedharan, A DFT based analysis of adsorption of Hg²⁺ ion on chitosan monomer and its citralidene and salicylidene derivatives: prior to the removal of Hg toxicity, *Int. J. Biol. Macromol.*, 99 (2017) 549–554.
- [2] K. Xia, R.Z. Ferguson, M. Losierb, N. Tchoukanovab, R. Brüningsc, Y. Djaoued, Synthesis of hybrid silica materials with tunable pore structures and morphology and their application for heavy metal removal from drinking water, *J. Hazard. Mater.*, 183 (2010) 554–564.
- [3] M. Dash, F. Chiellini, R.M. Ottenbrite, E. Chiellini, Chitosan—a versatile semi-synthetic polymer in biomedical applications, *Prog. Polym. Sci.*, 36 (2011) 981–1014.
- [4] H. Ueno, T. Mori, T. Fujinaga, Topical formulations and wound healing applications of chitosan, *Adv. Drug Delivery Rev.*, 52 (2001) 105–115.
- [5] R. Jayakumar, M. Prabakaran, P.T. Sudheesh Kumar, S.V. Nair, H. Tamura, Biomaterials based on chitin and chitosan in wound dressing applications, *Biotechnol. Adv.*, 29 (2011) 322–337.
- [6] P.K. Dutta, S. Tripathi, G.K. Mehrotra, J. Dutta, Perspectives for chitosan based antimicrobial films in food applications, *Food Chem.*, 114 (2009) 1173–1182.
- [7] B. Krajewska, Application of chitin- and chitosan-based materials for enzyme immobilizations: a review, *Enzyme Microb. Technol.*, 35 (2004) 126–139.
- [8] I. Kim, S. Seo, H. Moon, M. Yoo, I. Park, B. Kim, C. Cho, Chitosan and its derivatives for tissue engineering applications, *Biotechnol. Adv.*, 26 (2008) 1–21.
- [9] R. Pahwa, N. Saini, V. Kumar, K. Kohli, Chitosan-based gastroretentive floating drug delivery technology: an updated review, *Expert Opin. Drug Deliv.*, 9 (2012) 525–539.
- [10] Y. Chen, J. Wang, Preparation and characterization of magnetic chitosan nanoparticles and its application for Cu(II) removal, *Chem. Eng. J.*, 168 (2011) 286–292.
- [11] E.F.S. Vieira, A.R. Cestari, E. de B. Santos, F.S. Dias, Interaction of Ag(I), Hg(II), and Cu(II) with 1,2-ethanedithiol immobilized on chitosan: thermochemical data from isothermal calorimetry, *J. Colloid Interface Sci.*, 289 (2005) 42–47.
- [12] O.A.C. Monteiro Jr., C. Airolidi, Some studies of cross-linking chitosan–glutaraldehyde interaction in a homogeneous system, *Inter. J. Biol. Macromol.*, 26 (1999) 119–128.
- [13] W.S. Wan Ngah, S. Ab Ghani, A. Kamari, Adsorption behaviour of Fe(II) and Fe(III) ions in aqueous solution on chitosan and cross-linked chitosan beads, *Bioresour. Technol.*, 96 (2005) 443–450.
- [14] Rodrigo S. Vieira, Marisa M. Beppu, Interaction of natural and crosslinked chitosan membranes with Hg(II) ions, *Colloids Surf., A*, 279 (2006) 196–207.
- [15] M. Monier, D.M. Ayad, Y. Wei, A.A. Sarhan, Adsorption of Cu(II), Co(II), and Ni(II) ions by modified magnetic chitosan chelating resin, *J. Hazard. Mater.*, 177 (2010) 962–970.
- [16] W.S.W. Ngah, C.S. Endud, R. Mayanar, Removal of copper(II) ions from aqueous solution onto chitosan and cross-linked chitosan beads, *React. Funct. Polym.*, 50 (2002) 181–190.
- [17] L.S. Rocha, A. Almeida, C. Nunes, B. Henriques, M.A. Coimbra, C.B. Lopes, C.M. Silva, A.C. Duarte, E. Pereira, Simple and effective chitosan based films for the removal of Hg from waters: equilibrium, kinetic and ionic competition, *Chem. Eng. J.*, 300 (2016) 217–229.
- [18] R. Qu, Q. Liu, Preparation and adsorption properties for metal ions of chitosan crosslinked by PEG bisglycidyl ether, *Environ. Chem.*, 15 (1996) 41–46.
- [19] R. Qu, C. Wang, Studies on natural macromolecular adsorbents (x) synthesis and adsorption property of crosslinking chitosan resin, *Technol. Water Treat.*, 23 (1997) 230–236.
- [20] C. Wang, R. Qu, C. Sun, C. Ji, X. Zhou, G. Cheng, H. Huang, Studies on the synthesis and properties of CCTS/PVA/B-62 snake-cage type chelate membrane, *Ion Exch. Adsorpt.*, 20 (2004) 494–500.
- [21] C.X. Wang, M. Du, J.C. Lv, Q.Q. Zhou, Y. Ren, G.L. Liu, D.W. Gao, L.M. Jin, Surface modification of aramid fiber by plasma induced vapor phasegraft polymerization of acrylic acid. I. Influence of plasma conditions, *Appl. Surf. Sci.*, 349 (2015) 333–342.

- [22] J.M. García, F.C. García, F. Serna, J.L. de la Peña, High-performance aromatic polyamides, *Prog. Polym. Sci.*, 35 (2010) 623–686.
- [23] R. Ramani, T.M. Kotresh, R. Indu Shekar, F. Sanal, U.K. Singh, R. Renjith, G. Amarendra, Positronium probes free volume to identify para- and meta-aramid fibers and correlation with mechanical strength, *Polymer*, 135 (2018) 39–49.
- [24] V.B.C. Tan, X.S. Zeng, V.P.W. Shim, Characterization and constitutive modeling of aramid fibers at high strain rates, *Int. J. Impact Eng.*, 35 (2008) 1303–1313.
- [25] M.T. Islam, F. Aimone, A. Ferri, G. Rovero, Use of N-methylformanilide as swelling agent for meta-aramid fibers dyeing: kinetics and equilibrium adsorption of Basic Blue 41, *Dyes Pigm.*, 113 (2015) 554–561.
- [26] M.L. Sanyang, M. Yokasunderi, S.M. Sapuan, J. Sahari, Tea tree (*Melaleuca altemifolia*) fiber as novel reinforcement material for sugar palm biopolymer based composite films, *BioResources*, 12 (2017) 3751–3765.
- [27] M.L. Sanyang, S.M. Sapuan, M. Jawaid, M. R. Ishak, J. Sahari, Development and characterization of sugar palm starch and poly(lactic acid) bilayer films, *Carbohydr. Polym.*, 146 (2016) 36–45.
- [28] M. Mureseanu, A. Reiss, N. Cioatera, I. Trandafir, V. Hulea, Mesoporous silica functionalized with 1-furoyl thiourea urea for Hg(II) adsorption from aqueous media, *J. Hazard. Mater.*, 182 (2010) 197–203.
- [29] S. Kim, J. Lee, Miscibility and antimicrobial properties of m-aramid/chitosan hybrid composite, *Ind. Eng. Chem. Res.*, 52 (2013) 12703–12709.
- [30] J. Lee, R.M. Broughton, S.D. Worley, T.S. Huang, Antimicrobial polymeric materials; cellulose and m-aramid composite fibers, *J. Eng. Fibers Fabr.*, 2 (2007) 25–32.
- [31] M. Monier, Adsorption of Hg²⁺, Cu²⁺ and Zn²⁺ ions from aqueous solution using formaldehyde cross-linked modified chitosan-thioglyceraldehyde Schiff's base, *Int. J. Biol. Macromol.*, 50 (2012) 773–781.
- [32] H. Javadian, M. Ghaemy, M. Taghavi, Adsorption kinetics, isotherm, and thermodynamics of Hg²⁺ to polyaniline/hexagonal mesoporous silica nanocomposite in water/wastewater, *J. Mater. Sci.*, 49 (2014) 232–242.
- [33] I. Langmuir, The adsorption of gases on plane surfaces of glass, mica and platinum, *J. Am. Chem. Soc.*, 40 (1918) 1361–1403.
- [34] H.M.F. Freundlich, Über die adsorption in lösungen, *Zeitschrift für Physikalische*, 57 (1906) 385–470.
- [35] R. Qu, C. Sun, F. Ma, Y. Zhang, C. Ji, Q. Xu, C. Wang, H. Chen, Removal and recovery of Hg(II) from aqueous solution using chitosan-coated cotton fibers, *J. Hazard. Mater.*, 167 (2009) 717–727.
- [36] D.W. Hand, J.C. Crittenden, W.E. Thacker, User-oriented batch reactor solutions to the homogeneous surface diffusion model, *J. Environ. Eng.*, 109 (1983) 82–101.
- [37] G. McKay, The adsorption of basic dye onto silica from aqueous solution-solid diffusion model, *Chem. Eng. Sci.*, 39 (1984) 129–138.
- [38] P. Michard, E. Guibal, T. Vincent, P. Le Cloirec, Sorption and desorption of uranyl ions by silica gel: pH, particle size and porosity effects, *Microporous Mater.*, 5 (1996) 309–324.
- [39] E. Guibal, Interactions of metal ions with chitosan-based sorbents: a review, *Sep. Purif. Technol.*, 38 (2004) 43–74.
- [40] G.Z. Kyzas, E.A. Deliyanni, Mercury(II) removal with modified magnetic chitosan adsorbents, *Molecules*, 18 (2013) 6193–6214.
- [41] N.C. Braier, R.A. Jishi, Density functional studies of Cu²⁺ and Ni²⁺ binding to chitosan, *J. Mol. Struct. THEOCHEM*, 499 (2000) 51–55.
- [42] S. Lagergren, Zur theorie der sogenannten, adsorption gelöster stoffe, *Kungliga Svenska Vetenskapsakademiens, Handlingar*, 24 (1898) 1–39.
- [43] Y.S. Ho, G. McKay, Pseudo-second order model for sorption processes, *Process Biochem.*, 34 (1999) 451–465.
- [44] S. Azizian, Kinetic models of sorption: a theoretical analysis, *J. Colloid Interface Sci.*, 276 (2004) 47–52.